Astrocytes in the Optic Nerve Head of Glaucomatous Mice Display a Characteristic Reactive Phenotype

Rui Wang,[1,2] Philip Seifert,[2] and Tatjana C. Jakobs[2]

[1]The First Affiliated Hospital of Xi'an Jiaotong University, Xi'an, Shaanxi, China
[2]Department of Ophthalmology, Massachusetts Eye and Ear Infirmary/Schepens Eye Research Institute, Harvard Medical School, Boston, Massachusetts, United States

Correspondence: Tatjana C. Jakobs, Schepens Eye Research Institute, 20 Staniford Street, Boston, MA 02114, USA;
Tatjana_Jakobs@meei.harvard.edu.

Submitted: August 19, 2016
Accepted: January 11, 2017

Citation: Wang R, Seifert P, Jakobs TC. Astrocytes in the optic nerve head of glaucomatous mice display a characteristic reactive phenotype. *Invest Ophthalmol Vis Sci*. 2017;58:924–932. DOI:10.1167/iovs.16-20571

Purpose. Optic nerve head astrocytes, a subtype of white-matter astrocytes, become reactive early in the course of glaucoma. It was shown recently that in the DBA/2J mouse model of inherited glaucoma optic nerve astrocytes extend new longitudinal processes into the axon bundles before ganglion cell loss becomes apparent. The present study aims at testing whether this behavior of astrocytes is typical of early glaucomatous damage.

Methods. Mice expressing green fluorescent protein in individual astrocytes were used to evaluate the early response of astrocytes in the glial lamina of the optic nerve head after increasing the IOP using the microbead occlusion method. Tissue sections from the glial lamina were imaged consecutively by confocal and electron microscopy.

Results. Confocal and electron microscope images show that astrocytes close to the myelination transition zone in the hypertensive nerve heads extend new processes that follow the longitudinal axis of the optic nerve and invade axon bundles in the nerve head. Ultrastructurally, the longitudinal processes were largely devoid of subcellular organelles except for degenerating mitochondria.

Conclusions. The longitudinal processes are a common feature of glaucomatous optic nerve astrocytes, whereas they are not observed after traumatic nerve injury. Thus, astrocytes appear to fine-tune their responses to the nature and/or timing of the injury to the neurons that they surround.

Keywords: astrocytes, glial lamina, glaucoma, electron microscopy, confocal microscopy

A large body of evidence points to the optic nerve head (ONH) as a site of active tissue remodeling and retinal ganglion cell (RGC) axon damage in glaucoma. In humans and other primates the opening in the sclera that allows the ganglion cells' axons to exit the eye, is fortified by plates of collagenous tissue forming the lamina cribrosa, and pathologic changes of this structure have been reported in glaucoma.[1–6] In this region of the nerve the first signs of blockage of retrograde axonal transport occur.[7,8]

However, rodents do not have a true collagenous lamina cribrosa.[9–12] Yet, several rodent models of glaucoma, spontaneous and induced, exist and share many features with the human disease.[13–18] In humans, glaucomatous degeneration of retinal ganglion cells typically follows a sectorial pattern, and this feature is replicated in rodents.[19–22] Furthermore, in rats and mice, an elevation of IOP leads to blockage of axonal transport at the level of the ONH where ganglion cell axons run as discrete bundles with a topographic relationship to the retina.[12,23–26]

As apparently a collagenous lamina cribrosa is not necessary to develop glaucoma, the glial cells of the optic nerve have attracted attention as possible players in the pathophysiology. In the nerve head, the RGC axons are unmyelinated, but they are ensheathed by a dense meshwork of GFAP-positive astrocytes, the glial lamina.[10,12,27] Individual cells making up the glial lamina are relatively big and usually span at least half the diameter of the nerve, they overlap extensively, and their processes are oriented perpendicularly to the long axis of the nerve.[12,28]

In response to traumatic injury or glaucoma, the astrocytes become reactive and lose their typical arrangement, reorient or retract many of their processes, and become irregular in shape.[29–39] Using the DBA/2J model of inherited glaucoma, we recently demonstrated that astrocytes in the glial lamina grow out new longitudinal processes that invade the axon bundles rather than participating in forming the glial tubes around them.[38] These abnormal longitudinal processes appeared before there was detectable damage to the RGCs (at 6–7 months of age), but it was not clear what their function might be. We report an extension of our earlier study to the level of electron microscopy. We also have used the microbead occlusion model of ocular hypertension[18,40,41] rather than the DBA/2J strain. In the microbead model, the onset of the injury is defined more clearly in time and allows the study of very early changes in astrocyte morphology.

Materials and Methods

Animal Strains and Husbandry

All animal experiments were done according to the guidelines of the Association for Research in Vision and Ophthalmology (ARVO) Statement for the Use of Animals in Ophthalmic and Vision Research and were approved by the Institutional Animal

Care and Use Committee at the Schepens Eye Research Institute. We used hGFAPpr-GFP mice[42] that were backcrossed onto the C57bl/6 background. These mice express green fluorescent protein (GFP) in individual astrocytes in the optic nerve and other parts of the central nervous system (CNS).[12,42,43] The strain was maintained in heterozygous state and was backcrossed in each generation to C57bl/6 (obtained from the Jackson Laboratories, Bar Harbor, ME, USA) to avoid genetic drift. Individual animals were tested for GFP expression by inspecting ear snips under a fluorescent microscope.[38] Male and female mice of 2 to 8 months were used for all experiments.

Microbead Injection

Ocular hypertension was induced by the injection of microbeads (15 μm diameter; Invitrogen, Carlsbad, CA, USA) into the anterior chamber of the right eye, essentially as described by the developers of the method.[18,40,41] Another group of mice was injected unilaterally with 2 to 3 μl sterile saline solution as an additional control. Intraocular pressure was measured under isoflurane anesthesia in both eyes one time before and twice weekly after injection with a rebound tonometer (TonoLab; iCare, Espoo, Finland). All measurements were taken at the same time in the morning to minimize circadian variation in IOP. The cumulative IOP (cIOP) was calculated for each eye as the area under the curve of IOP over time with a user-written Matlab (Mathworks, Natick, MA, USA) routine.[44]

Tissue Preparation and Embedding

The head with the eyes and optic nerves in situ were fixed for 2 hours in 4% paraformaldehyde. Retinas and optic nerves were dissected from the surrounding tissue as described previously.[12,45] Optic nerves were detached from the retina, embedded in 6% agarose, and sectioned at 100 μm, or 200 μm (when electron microscopy was performed after confocal imaging) in transverse orientation using a vibratome (Leica VT1000 S; Leica Microsystems, Buffalo Grove, IL, USA) and mounted with Vectashield (Vector Laboratories, Burlingame, CA, USA). For retinal ganglion cell counting, retinas were whole-mounted on AA nitrocellulose filters (MF19; Millipore, Billerica, MA, USA). Imaging of optic nerve astrocytes and immunostained retinas was done within a week after preparation of the samples.

Confocal Microscopy and Image Reconstruction

Images of astrocytes in the unmyelinated segment of the optic nerve were obtained on a Leica TCS SP8 confocal microscope using a ×63 glycerol immersion objective. Individual agarose sections were kept in order starting from 1 (at the level of the sclera to 100 μm behind the sclera) to 4 (300–400 μm behind the sclera). We restricted the analysis to the glial lamina, and astrocytes in the optic nerve proper (myelinated portion) were not imaged. Image stacks were taken through the whole extent of the cell. Image size was 1024 × 1024 pixels in x/y, corresponding to a resolution of 0.1805 μm per pixel. The z step size was 0.33 μm. The 3D reconstruction of astrocytes was accomplished using a volume visualization program (Amira; Visage Imaging, San Diego, CA, USA).

Transmission Electron Microscopy

After confocal microscopy the optic nerve sections with the surrounding agarose were immediately immersion fixed with half strength Karnovsky's fixative for 2 hours at room temperature. The agarose section was sandwiched between two filters to help stabilizing and handling the delicate tissue. The samples were processed for electron microscopy and imaged using a FEI Tecnai G2 Spirit transmission electron microscope (FEI, Hillsboro, OR, USA) at 80 kV equipped with an AMT XR41 digital CCD camera (Advanced Microscopy Techniques, Woburn, MA, USA). A complete description of the tissue preparation procedure is given in the Supplementary Methods.

Immunohistochemistry

Whole-mounted retinas were incubated in primary antibodies for 3 to 4 days at 4°C. The primary antibodies used were: rabbit anti-β-III tubulin (1:200; Cell Signaling Technology, Danvers, MA, USA), mouse anti-Brn3a (1:200, Nippon Chemi-Con, Tokyo, Japan). Secondary antibodies were FITC-conjugated donkey anti-rabbit IgG, and rhodamine-conjugated donkey anti-mouse IgG (both from Jackson Immunoresearch Laboratories, Inc., West Grove, PA, USA). Retinas were counterstained with the nuclear dye DAPI (Life Technologies, Grand Island, NY, USA), and mounted in Vectashield.

Ganglion Cell Counting

Retinal ganglion cells were counted on whole-mounted retinas after immunostaining for Brn3a and β-III tubulin. The images were acquired with a ×63 glycerol immersion objective on a Leica TCS SP8 confocal microscope. The retina was divided into quadrants and two midperipheral regions (defined as equidistant to the ONH and the border of the retina) were imaged in every quadrant (8 regions of 184.52 μm by 184.52 μm per retina). To include all cells in the ganglion cell layers, z-stacks were taken through the ganglion cell layer at a step size of 0.5 μm, and maximum-intensity projections of these stacks were made in ImageJ. All cells in the ganglion cell layer that colocalized with anti-β-III tubulin and anti-Brn 3a were counted and the ganglion cell density per retina was calculated. Cells positive for β-III tubulin were counted manually by individuals blinded to different groups of the animal using ImageJ (National Institute of Health [NIH], Bethesda, MD, USA), Brn3a-positive cells were counted semiautomatically in a user-written Matlab routine (version R2013b). Differences in RGC counts were tested for significance using Student's *t*-test.

Cell Tracing

Every animal received a number code after the experiment and the investigator performing morphometric measurements and statistical analysis was ignorant of the IOP history of the eye. Unprocessed confocal image stacks through the glial lamina were imported to ImageJ. To quantify longitudinal processes individual astrocytes were traced using the Simple Neurite Tracer plugin.[46] Image stacks containing more than 10 labeled cells were not analyzed because in these cases it was impossible to discern individual cells. For examples of digitized astrocytes, see Supplementary Figure S1. The length of all processes (transverse and longitudinal) was measured for each cell and the ratio of longitudinal process length to total process length (L/T) was calculated. Differences between groups were tested for significance using Kruskal-Wallis and Wilcoxon rank sum tests. All statistical tests were done in Matlab.

Data Sharing

All original unprocessed images and image stacks were deposited in the Harvard Dataverse and are accessible in the

Investigative Ophthalmology & Visual Science

public domain under https://dataverse.harvard.edu/dataverse/Astrocytes_Glaucoma.

Results

Elevation of IOP Induced by Microbead Injection Into Anterior Chamber

We injected 27 GFP-positive hGFAPpr-GFP mice unilaterally with microbeads. The mice were 6 to 8 months of age at the beginning of the experiment because we first observed longitudinal processes in the astrocytes of DBA/2J mice at that age.[38] Four mice were excluded from the study because they showed corneal opacities that did not resolve within days after the injection. The contralateral eye was left untreated. Recently, it was demonstrated that elevation of the IOP in one eye leads to glial cell activation in the contralateral eye, and in some mouse strains, even to RGC loss.[47–50] Therefore, the contralateral eye cannot be considered truly "normal." Therefore, we included 8 naïve mice age matched to the microbead-injected mice at the end of the experiment (i.e., 8–9 months old) as controls. A second control group consisted of 9 young animals (3 months) to determine whether age alone has an influence on astrocyte morphology. We also injected another group of 8 young adult mice unilaterally with sterile saline solution to exclude the possibility that any manipulation of the eye may cause glial activation or ganglion cell loss. The IOP was measured every 3 or 4 days in the following 4 weeks after surgery (Supplementary Figs. S2A, S2B).

Due to the variability of the level and duration of IOP changing between individual animals, we used the cumulative IOP, defined as the area under the curve of IOP over time, measured in mm Hg days.[44] However, as we did not use the contralateral eye as the "normal" control, we calculated the cIOP for each eye rather than the difference in cIOP between the injected and contralateral eyes. The cIOP was 479.6 ± 44.58 mm Hg days (mean ± SD, $n = 23$) for the microbead-injected eyes, which was higher than for the contralateral eyes (410.8 ± 46.82, $P < 0.001$, t-test, Fig. 1A). For the sham operated group (saline injection), there was no significant difference in the cIOP comparison between saline injected eyes (300.4 ± 12.26, $n = 8$) and contralateral eyes (312.6 ± 23.5, $n = 8$, $P = 0.21$, Fig. 1B). The maximum IOP for the microbead group was 23.7 ± 3.16 mm Hg (mean ± SD, $n = 23$), which was higher than in the contralateral group (19.5 ± 3.07, $n = 23$, $P < 0.001$, Fig. 1C). We also noticed that the IOP in the contralateral eyes of the old mice was higher than baseline (15.16 ± 0.96 mm Hg in the contralateral eyes versus the baseline of 12.08 ± 1.6 mm Hg, $P < 0.01$). There was no significant difference in maximum IOP between saline injected eyes (13.6 ± 0.9) and contralateral eyes (14.5 ± 1.8, $n = 8$, $P = 0.12$, Fig. 1D).

Ganglion Cell Loss After IOP Elevation

Brn3a and β-III tubulin were used to assess RGC loss (Figs. 2A–I). We compared the RGC densities obtained from these two antibodies in 10 retinas. The RGC number was 8.58% ± 2.8% lower estimated by Brn3a staining rather than by β-III tubulin staining, but the differences between these two counting methods were consistent (Fig. 2J).

We first determined the RGC density (by staining for Brn3a) in a group of age-matched naïve mice that had no procedures performed on them as a baseline value. The RGC density in this group was 4135 ± 333 cells/mm^2 ($n = 8$). The RGCs densities

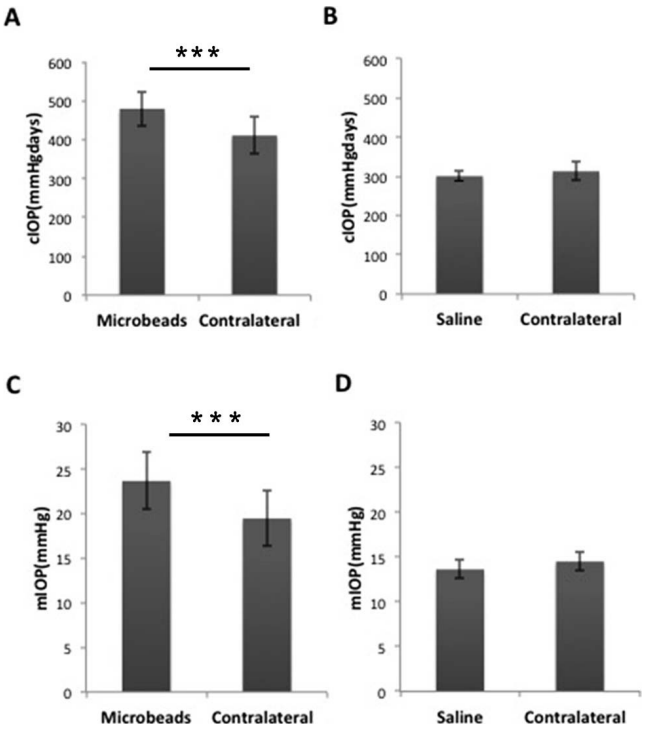

Figure 1. Comparison of two evaluation indices of IOP in different groups. (**A**) Cumulative IOPs (the area under the curve of IOP over time) were significantly different between microbead-injected eyes and their contralateral eyes. (**B**) Cumulative IOPs were similar in the saline-injected eyes and their contralateral eyes. (**C**) Maximum IOPs (mIOPs; maximum IOP during the whole recording period) were significantly different between microbead-injected eyes and their contralateral eyes. (**D**) Maximum IOPs were similar in the saline-injected eyes and their contralateral eyes. Data are presented as mean ± SD. ***$P < 0.001$ (t-test).

in the eyes that received microbead injections ($n = 23$) were significantly lower than those of the contralateral eyes (3835 ± 363 vs. 4170 ± 242 cells/mm^2, $P < 0.001$, Fig. 2K). There was no significant difference between the naïve eyes and the contralateral eyes, suggesting that unilateral microbead injection did not cause RGC loss in the contralateral eye in this strain. RGC loss was only slightly correlated with cIOP ($R^2 < 0.1$).

We also injected a group of young (2 months) mice unilaterally with sterile saline solution. There was no RGC loss in the injected eye in this group (4650 ± 181 vs. 4726 ± 298 cells/mm^2, not significant, Fig. 2L). The overall higher RGC density in the younger mice is consistent with the observation that mice spontaneously lose cells with age, even without the presence of glaucoma.[19]

Longitudinal Astrocytic Processes in the Glial Lamina

Though the shape of the astrocytes in the glial lamina is fairly stereotypical, the cells are quite complex. To quantify cell morphologies, we digitally traced all astrocytes in the sample that were well-isolated enough from neighboring labeled cells to unambiguously identify their processes. Two sets of strain-matched naïve mice served as controls. First, we used 3-month-old animals and traced 30 individual astrocytes from 11 nerves to establish the baseline morphology of normal ONH astrocytes. However, morphologic changes might occur with normal aging, so we additionally traced 24 astrocytes from 6

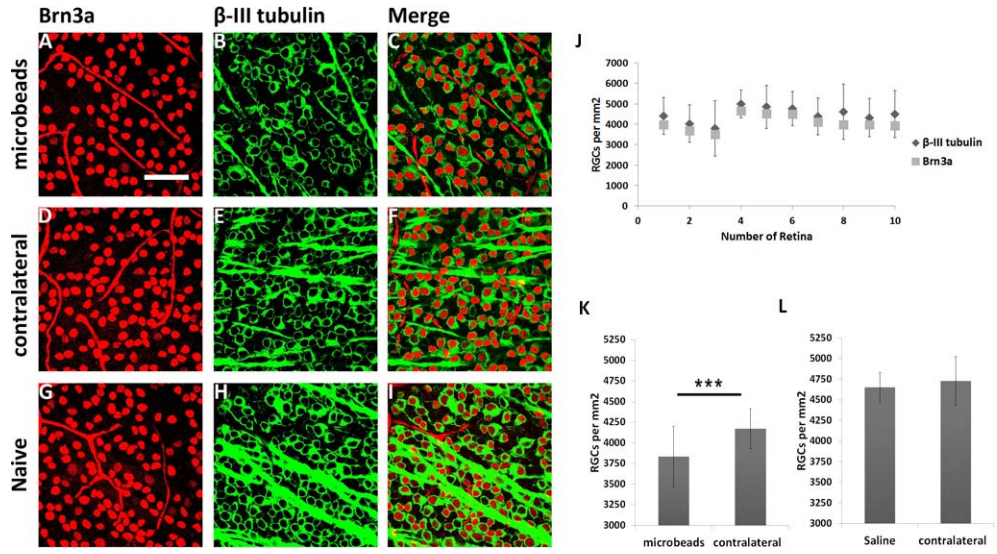

Figure 2. Ganglion cell loss after microbead injection. (**A**, **D**, **G**) Mouse anti-Brn3a antibody labeled ganglion cells in microbead-injected eyes, their contralateral eyes, and aged-matched naïve eyes. (**B**, **E**, **H**) Rabbit anti β-III tubulin antibody labeled ganglion cells in microbead-injected eyes, their contralateral eyes and aged-matched naïve eyes. (**C**, **F**, **I**) Merged images show double labeled ganglion cells in all three groups. *Scale bar*: 20 μm. (**J**) Comparison of ganglion cell densities obtained from mouse anti-Brn3a antibody labeling and rabbit anti β-III tubulin antibody labeling in 10 whole mount retinas. The ganglion cell densities obtained from Brn3a staining were relatively lower estimated than β-III tubulin staining, but the differences between these two counting methods were consistent. All images represent maximum-intensity projections of image stacks through the ganglion cell layer, taken at a z-step size of 0.5 μm. (**K**) Ganglion cell densities in microbead-injected eyes were significant lower than those in the contralateral eyes. (**L**) Ganglion cell densities were similar in the saline-injected eyes and their contralateral eyes. $N = 23$ (**B**), $n = 8$ (**C**). $^{***}P < 0.001$ (*t*-test). Data are presented as mean values ± SD.

nerves at 8 to 9 months to serve as strain- and age-matched controls for the microbead injected eyes. In all cases, the unmyelinated region was subdivided into 100 μm sections beginning at the sclera (region 1) to the myelination transition zone (region 4). Sections at more than 400 μm behind the sclera contained myelinated optic nerve and were not imaged. Figure 3 shows typical ONH astrocytes from the naïve B6.hGFAPpr-GFP mice at 3 (Figs. 3A–D) and 8 to 9 (Figs. 3E–G) months by regions 1 to 4. The processes of astrocytes from naïve optic nerves are long and smooth, spanning over half the diameter of the optic nerve. Three-dimensional reconstruction shows that the whole astrocyte is slightly concave, with most of the processes oriented transversely to the long axis of optic nerve—the typical morphology of astrocytes in the glial lamina.[12] There are numerous processes emanating mostly from the cell body and the proximal segments of the main processes (arrows in Fig. 3), but as shown in 3D reconstructions, very few longitudinal processes are present in naïve astrocytes (Fig. 3). There was no difference between the astrocytes from the young and old animals. The total process length was 1140.34 ± 459.44 μm for the 3-month group and 994.73 ± 345.52 μm for the 8- to 9-month group (not significant). The L/T ratio (length of all longitudinal processes divided by total process length) was 0.0316 (range, 0–0.0874) for young and 0.0248 (range, 0–0.0944) for old animals (not significant). This indicates that the growth of longitudinal processes is not driven by age alone.

The astrocytes from the microbead-injected group showed obvious morphologic changes (Figs. 4C–E) and delicate longitudinal processes were found to grow out from the regular processes (Fig. 4D'). In the sample of 45 astrocytes, originating from 14 microbead-injected eyes, the total process length was similar to the naïve controls (1193.87 ± 478.97), but L/T was 0.0639 (range, 0–0.1976) for astrocytes after microbead injection ($P < 0.05$, compared to the age-matched control group). We next correlated the individual L/T ratios for each cell with the position in the optic nerve where the cell was localized. As shown in Figure 5A, astrocytes in the initial 200 μm behind the sclera, rarely had longitudinal processes. Closer to the myelination transition zone (200–400 μm) these processes were far more common. We next tested whether the presence of longitudinal processes correlates with RGC loss. For this, each of the 14 nerves was treated as one biologic replicate since all cells in the same nerve were presumably subject to the same pressure insult and ganglion cell loss. As longitudinal processes rarely occurred in the initial 200 μm, only cells from 200–400 μm were considered. In those cases we had more than one traced astrocyte per nerve their L/T ratios were averaged. The L/T ratios correlated with RGC loss ($R^2 = 0.41$, Fig. 5B). There was no obvious difference between nerves from male and female mice (Fig. 5B).

Finally, we asked whether longitudinal processes only occurred in old eyes with ocular hypertension. Therefore, as an additional control, we injected 3 young B6.hGFAPpr-GFP mice with microbeads and digitized 8 astrocytes from their glial laminas 200 to 400 μm behind the sclera. Total process length in the young injected cells was similar to the naïve controls (1029 ± 179.75 μm, not significant), but the L/T ratio was higher (0.0868; range, 0.0097–0.2518, $P < 0.05$). Taken together, these findings indicate that the growth of longitudinal processes is likely driven by the increase in IOP or ganglion cell distress and are a common feature of reactive astrocytes in the optic nerve regardless of age.

Transmission Electron Microscopy

We imaged individual astrocytes in 200 μm agarose sections of the ONH 1 month after microbead injection with confocal microscopy to verify that longitudinal processes were present. Afterwards, we used the same tissue to generate thin sections for electron microscopy to inspect the relationship between newly formed processes and ganglion cell axon bundles. Longitudinal processes should be identifiable because their intermediate filaments will be sectioned transversely (and,

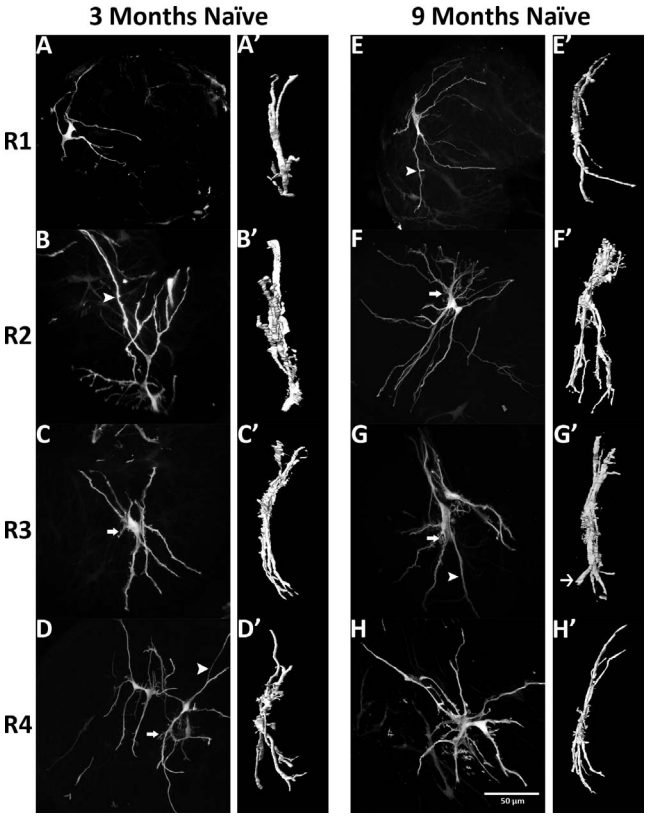

Figure 3. Typical ONH astrocytes from naïve B6.hGFAPpr-GFP mice. (**A**–**D**) Astrocytes obtained from ONHs of 3 months naïve mice. (**A**'–**D**') Three-dimensional reconstructions of the astrocytes in (**A**–**D**). (**E**–**H**) Astrocytes obtained from ONH of 9-month naïve mice. (**E**'–**H**') Three-dimensional reconstructions of astrocytes in (**E**–**H**). The processes are long and smooth (*arrowheads* in [**B**–**E**, **G**]). There are numerous fine processes emanating mostly from the cell body and the proximal segments of the main processes (*arrows* in [**C**, **D**, **F**, **G**]). Only occasionally there are processes in the longitudinal direction in naïve ONH astrocytes (*arrow* in [**G**']) R1, region 1, 0 to 100 µm behind the sclera; R2, region 2, 100 to 200 µm behind the sclera; R3, 200 to 300 µm behind the sclera; R4, 300 to 400 µm behind the sclera. *Scale bar*: 50 µm.

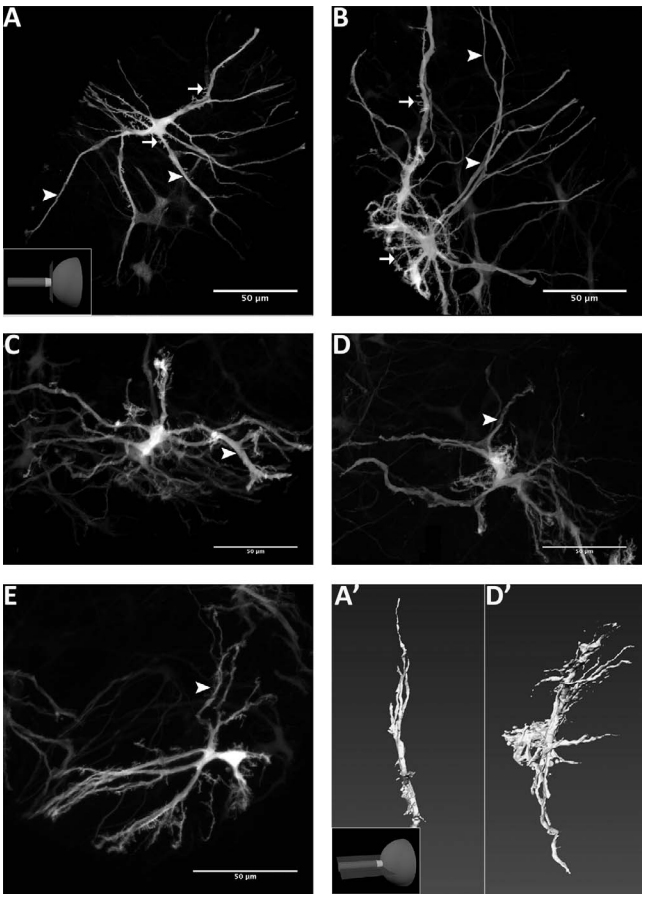

Figure 4. Green fluorescent protein–positive astrocytes in the ONH from naïve, contralateral, and microbead-injected eyes. (**A**, **B**) Typical ONH astrocytes from the naïve (**A**) and the contralateral (**B**) eyes. The processes of astrocytes from naïve optic nerves are long and smooth (*arrowheads*), spanning over half the diameter of the optic nerve. There are numerous very short processes emanating mostly from the cell body and the proximal segments of the main processes (*arrows*). (**C**–**E**) Optic nerve head astrocytes from the microbead-injected eyes. Some processes became thicker (*arrowheads*). (**A**') Three-dimensional reconstruction of astrocyte in (**A**). The whole astrocyte is fairly flat, slightly concave, with most of the processes oriented transversely to the long axis of the optic nerve. Very few longitudinal processes are present in naïve astrocyte. (**D**') Three-dimensional reconstruction of astrocyte in (**D**). A large number of longitudinal processes were found to grow out from the processes of ONH astrocytes. The schematics in (**A**) and (**A**') indicate the plane of section. *Scale bar*: 50 µm.

thus, appear as puncta) rather than longitudinally, as in the regular astrocyte processes that form the glial tubes.[51] Furthermore, profiles of longitudinal processes should occur in the middle of axon bundles. Following these rules, we detected numerous profiles of longitudinal processes in the ONH from microbead-injected eyes (Figs. 6A, 6B). The longitudinal processes did not contain subcellular organelles, but often electron-dense inclusion bodies were present that were surrounded by a membrane. Higher magnification images showed that these were degenerating mitochondria (Figs. 6A', 6B'). In ONHs after microbead injection, we also observed vacuoles of different shapes and sizes (Fig. 7A). Some of these vacuoles seemed to be adjacent to a longitudinal process (Fig. 7B). Though most of the ganglion cell axons appeared morphologically normal, the space between single axons was loosened, and the astrocytes grew out numerous small processes between the axons (Figs. 7C–E). In some axons we observed abnormally large mitochondria or mitochondria with very few cristae (Fig. 7F). Neither longitudinal processes nor vacuoles were found in naïve optic nerves from young mice (Figs. 6C, 6D). The axons within each bundle were tightly packed with very few astrocyte processes that invaded the bundles (Fig. 6C). Axonal mitochondria always had visible cristae (Fig. 6D).

Comparison of Glaucomatous Optic Nerves With Aged Optic Nerves

In electron microscopy, our primary control for a normal ONH were young (3 months old), nonglaucomatous C57bl/6 mice. However, mice lose RGCs spontaneously with age,[19] and some of the pathologic changes we observed in our experimental animals may be related to age rather than to an elevation in IOP. Therefore, we used the optic nerves from a naïve 6-month-old C57bl/6 mouse, prepared in exactly the same way as described above, as an additional control. In these older nerves, we did not observe either longitudinal processes or vacuoles (Fig. 6E). However, several of the axons contained abnormal mitochondria (Fig. 6F).

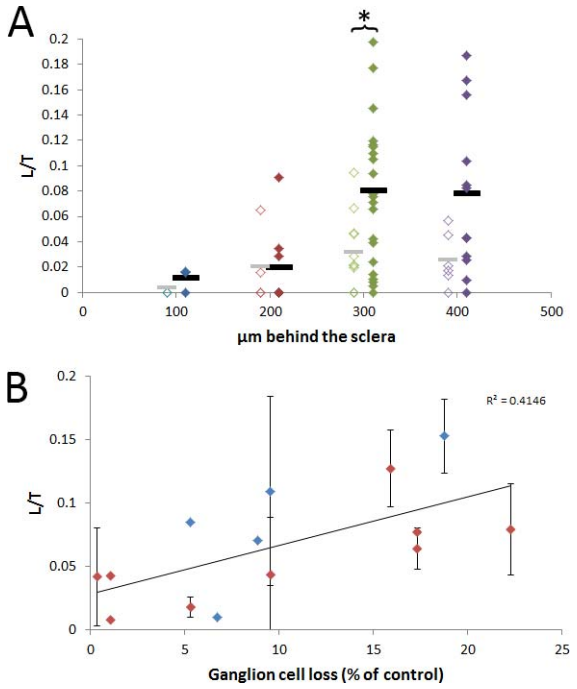

Figure 5. Longitudinal processes in ONH astrocytes. (**A**) Longitudinal processes were fairly rare in the initial 200 µm behind the sclera. The L/T ratios are given for every 100 µm segment. *Filled dark blue*, 0 to 100 µm, $n = 3$ cells; *red*, 100 to 200 µm, $n = 8$; *green*, 200 to 300 µm, $n = 22$; *violet*, 300 to 400 µm, $n = 12$. *Black bars* represent group means. *Open symbols* represent L/T ratios of age- and strain-matched naïve control cells ($n = 3$, $n = 4$, $n = 11$, $n = 6$ for the four regions, respectively). *Gray bars* represent group means for the naïve cells. *$P < 0.05$, Wilcoxon rank sum test. (**B**) Correlation of L/T rations versus retinal ganglion cell loss (in %). *Blue symbols* represent nerves from male mice; *red symbols* represent nerves from female mice. Data are presented as mean values ± SD.

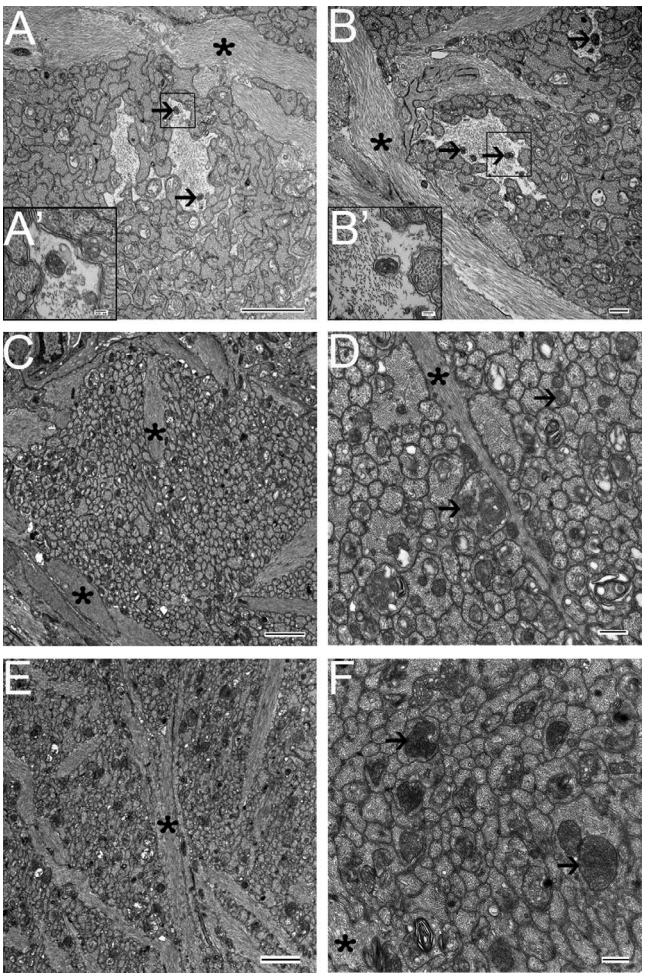

Figure 6. Electron microscopy of the ONH from microbead-injected eyes and naïve eyes. (**A**, **B**) Optic nerve head after microbead injection. Regular astrocyte processes (*asterisks*) with intermediate filaments. The longitudinal processes can be identified by the orientation of their intermediate filaments and the lack of continuity with the other processes. There are two longitudinal processes in the middle of the axon bundle in (**A**) and two longitudinal processes (a big one in the *lower left* and a small one in *upper right*) in the middle of the axon bundle in (**B**). *Arrows* point to materials in the longitudinal processes. (**A'**, **B'**) The insert shows a high-power image of the region corresponding to the *black box* in (**A**) and (**B**). The materials inside the longitudinal processes are degenerating mitochondrion, with some cristae still visible. (**C**–**F**) Optic nerve head of a 3-month-old naïve mouse (**C**, **D**) and of a 6-month-old naïve mouse (**E**, **F**). *Asterisks* indicate regular astrocyte processes that form the glia tube. No longitudinal processes were found. The axons within each bundle were tightly packed with very few astrocyte processes that invaded the bundles (**C**, **E**). Axonal mitochondria (*arrows* in [**D**]) in 3-months-old ONH always had visible cristae. Some axons in 6-months-old ONH contained abnormal mitochondria (*arrows* in [**F**]). *Scale bars*: 2 µm (**A**, **C**, **E**), 500 nm (**B**, **D**, **F**), 200 nm (**A'**, **B'**).

Discussion

In an earlier study, we reported that astrocytes from the ONH extend new longitudinal processes into the axon bundles in 6- to 8-month-old DBA/2J mice.[38] The changes in the optic nerve preceded overt RGC loss, and were the first obvious signs of reactivity we observed in astrocytes. However, there are two caveats about our earlier study. First, the observations were made in DBA/2J mice. DBA/2J is a valuable model of glaucoma,[16] but it differs from other rodent models of glaucoma in terms of gene expression,[33,36,37,52] and its reaction to radiation treatment.[53–56] A possible reason may be the pronounced inflammatory component of DBA/2J glaucoma.[57] Given the differences between rodent glaucoma models, generalizations from one of them to glaucoma in general must be treated with caution. Second, in our earlier study, we did not use electron microscopy and, therefore, were unable to obtain more details about the relationship between these newly formed longitudinal processes and injured optic nerve axons.

Using unilateral microbead injection in B6.hGFAPpr-GFP mice, we asked whether longitudinal processes are a common feature of glaucomatous optic nerve rather than a peculiarity of the DBA/2J strain. In our cohort of 7- to 8-month-old mice, microbead injection led to a significant increase in cIOP. However, we noted that the IOP in the contralateral eye in these older mice is higher than in younger animals, agreeing with previous reports.[58] Older mice on the C57bl/6 background have been shown to be less vulnerable to ganglion cell loss in the microbead model than their younger counterparts or mice of other strains.[44] We did observe a significant, albeit moderate, loss of RGCs in the microbead injected eyes; however, the loss was poorly correlated to the pressure insult the eye had sustained. A possible explanation for this observation might be that taking IOP measurements twice per week does not truly reflect the IOP history of the eye during the observation period and misses events of elevated IOP or pressure spikes[44] that may be detectable only by continuous telemetry.[59] In addition, even in inbred strains individual differences in the vulnerability of RGCs to IOP may exist.

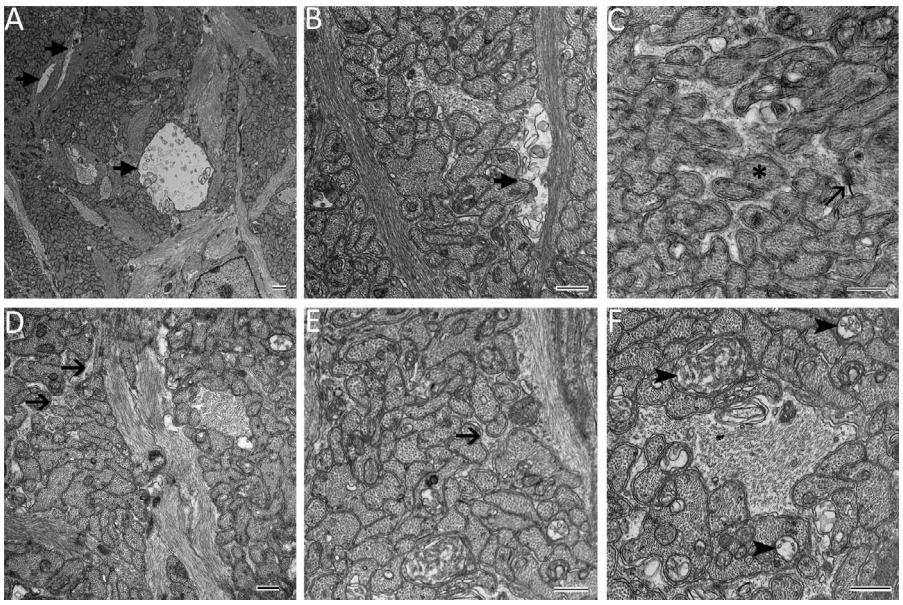

Figure 7. Other morphologic changes in ONH of microbead-injected eyes. (**A**, **B**) Vacuoles of different shapes and size that seem to be fluid-filled and sometimes contain debris (*arrows* in [**A**]). Some of these vacuoles were adjacent to the longitudinal processes (*arrows* in [**B**]). (**C**) Small processes are interspersed between axons and sometimes encircle individual axons or small groups of axons (*asterisk*). The *arrow* points to a connection between small neighboring astrocyte processes. (**D**, **E**) The space between single axons was loosened, and the astrocytes grew out many small processes (*arrows* in [**D**] and [**E**]) in between the axons. (**F**) Abnormally large mitochondria or mitochondria with very few cristae in ONH axons (*arrowheads*) after microbead injection. *Scale bar*: 500 nm.

We observed longitudinal processes similar to those that are present in DBA2/J nerves after microbead injection, indicating that they are a common feature of glaucomatous optic nerve astrocytes. This behavior is not found in protoplasmic astrocytes after a stab wound to the gray matter, where the astrocytes occupy nonoverlapping spatial domains which are maintained even after injury.[60,61] Nor is it observed after severe traumatic injury in the astrocytes of the glial lamina and the optic nerve proper.[35] Glaucoma leads to slow, but progressive, RGC damage, and the astrocytes may react to this type of injury in a unique way.

The presence of the longitudinal processes depended on the localization of the cell within the unmyelinated segment of the nerve: closer to the myelination transition zone more longitudinal processes were encountered. This may be an indication of phagocytic activity in these cells, as astrocytes in the myelination transition zone are active phagocytes.[62] Ultrastructurally, the longitudinal processes contain sparse intermediate filaments and no subcellular organelles other than apparently degenerating mitochondria. Davis et al.[63] recently suggested that optic nerve astrocytes aid in the transcellular degradation of axonal mitochondria, and the mitochondria in the longitudinal processes may be of axonal origin.

Compared to the normal ONH, the space between single axons appears loose after IOP elevation, and fine astrocytic processes intermingle with the unmyelinated axons, sometimes encircling single axons. Recent studies identified decreased axon packing and an increase in astrocyte processes for the myelinated portion of the optic nerve, also.[64,65] One of these studies also reported a loss of axonal mitochondria in glaucomatous nerves before overt degeneration[64] and abnormal mitochondria accumulate in the axons of glaucomatous DBA/2J mice.[66] Thus, an imbalance of energy production and metabolic demand of the RGCs, particularly in the aging nerve, may be an important factor in ganglion cell degeneration.[67–69]

We hypothesized that newly formed astrocyte processes are attracted to distressed axons by signals that are as yet unknown. As in the spinal cord, one of their functions may be to surround and limit the spread of axonal damage. The processes also may be phagocytic and possibly relieve the axons of degenerating mitochondria. Finally, astrocytes may be involved in clearing the debris of axons that did eventually degenerate and die.

Acknowledgments

The authors thank Elio Raviola and Frederic Jakobiec for advice on electron microscopy; and Richard Masland, Daniel Sun, and Anthony Pappas for critically reading the manuscript.

Supported by NIH Grants 2R01EY019703 and R01EY022092, the NIH Core Grant for vision research P30EY003790, and grants from the Chinese Scholarship Council and Research to Prevent Blindness.

Disclosure: **R. Wang**, None; **P. Seifert**, None; **T.C. Jakobs**, Santen, Inc. (R)

References

1. Jonas JB, Berenshtein E, Holbach L. Anatomic relationship between lamina cribrosa, intraocular space, and cerebrospinal fluid space. *Invest Ophthalmol Vis Sci*. 2003;44:5189–5195.
2. Yang H, Williams G, Downs JC, et al. Posterior (outward) migration of the lamina cribrosa and early cupping in monkey experimental glaucoma. *Invest Ophthalmol Vis Sci*. 2011;52:7109–7121.
3. Strouthidis NG, Fortune B, Yang H, Sigal IA, Burgoyne CF. Effect of acute intraocular pressure elevation on the monkey optic nerve head as detected by spectral domain optical coherence tomography. *Invest Ophthalmol Vis Sci*. 2011;52:9431–9437.
4. Kiumehr S, Park SC, Syril D, et al. In vivo evaluation of focal lamina cribrosa defects in glaucoma. *Arch Ophthalmol*. 2012;130:552–559.

5. Sigal IA, Wang B, Strouthidis NG, Akagi T, Girard MJ. Recent advances in OCT imaging of the lamina cribrosa. *Br J Ophthalmol*. 2014;98(suppl 2):ii34–ii39.
6. Burgoyne CF. A biomechanical paradigm for axonal insult within the optic nerve head in aging and glaucoma. *Exp Eye Res*. 2011;93:120–132.
7. Quigley HA, Addicks EM. Chronic experimental glaucoma in primates. II. Effect of extended intraocular pressure elevation on optic nerve head and axonal transport. *Invest Ophthalmol Vis Sci*. 1980;19:137–152.
8. Pease ME, McKinnon SJ, Quigley HA, Kerrigan-Baumrind LA, Zack DJ. Obstructed axonal transport of BDNF and its receptor TrkB in experimental glaucoma. *Invest Ophthalmol Vis Sci*. 2000;41:764–774.
9. Morrison J, Farrell S, Johnson E, Deppmeier L, Moore CG, Grossmann E. Structure and composition of the rodent lamina cribrosa. *Exp Eye Res*. 1995;60:127–135.
10. Morcos Y, Chan-Ling T. Concentration of astrocytic filaments at the retinal optic nerve junction is coincident with the absence of intra-retinal myelination: comparative and developmental evidence. *J Neurocytol*. 2000;29:665–678.
11. May CA, Lutjen-Drecoll E. Morphology of the murine optic nerve. *Invest Ophthalmol Vis Sci*. 2002;43:2206–2212.
12. Sun D, Lye-Barthel M, Masland RH, Jakobs TC. The morphology and spatial arrangement of astrocytes in the optic nerve head of the mouse. *J Comp Neurol*. 2009;516:1–19.
13. Morrison JC, Moore CG, Deppmeier LM, Gold BG, Meshul CK, Johnson EC. A rat model of chronic pressure-induced optic nerve damage. *Exp Eye Res*. 1997;64:85–96.
14. Morrison JC, Johnson E, Cepurna WO. Rat models for glaucoma research. *Prog Brain Res*. 2008;173:285–301.
15. John SW, Smith RS, Savinova OV, et al. Essential iris atrophy, pigment dispersion, and glaucoma in DBA/2J mice. *Invest Ophthalmol Vis Sci*. 1998;39:951–962.
16. Libby RT, Anderson MG, Pang IH, et al. Inherited glaucoma in DBA/2J mice: pertinent disease features for studying the neurodegeneration. *Vis Neurosci*. 2005;22:637–648.
17. McKinnon SJ, Schlamp CL, Nickells RW. Mouse models of retinal ganglion cell death and glaucoma. *Exp Eye Res*. 2009; 88:816–824.
18. Sappington RM, Carlson BJ, Crish SD, Calkins DJ. The microbead occlusion model: a paradigm for induced ocular hypertension in rats and mice. *Invest Ophthalmol Vis Sci*. 2010;51:207–216.
19. Danias J, Lee KC, Zamora MF, et al. Quantitative analysis of retinal ganglion cell (RGC) loss in aging DBA/2NNia glaucomatous mice: comparison with RGC loss in aging C57/BL6 mice. *Invest Ophthalmol Vis Sci*. 2003;44:5151–5162.
20. Jakobs TC, Libby RT, Ben Y, John SW, Masland RH. Retinal ganglion cell degeneration is topological but not cell type specific in DBA/2J mice. *J Cell Biol*. 2005;171:313–325.
21. Schlamp CL, Li Y, Dietz JA, Janssen KT, Nickells RW. Progressive ganglion cell loss and optic nerve degeneration in DBA/2J mice is variable and asymmetric. *BMC Neurosci*. 2006;7:66.
22. Soto I, Pease ME, Son JL, Shi X, Quigley HA, Marsh-Armstrong N. Retinal ganglion cell loss in a rat ocular hypertension model is sectorial and involves early optic nerve axon loss. *Invest Ophthalmol Vis Sci*. 2011;52:434–441.
23. Johansson JO. Inhibition of retrograde axoplasmic transport in rat optic nerve by increased IOP in vitro. *Invest Ophthalmol Vis Sci*. 1983;24:1552–1558.
24. Johansson JO. Retrograde axoplasmic transport in rat optic nerve in vivo. What causes blockage at increased intraocular pressure? *Exp Eye Res*. 1986;43:653–660.
25. Johansson JO. Inhibition and recovery of retrograde axoplasmic transport in rat optic nerve during and after elevated IOP in vivo. *Exp Eye Res*. 1988;46:223–227.
26. Salinas-Navarro M, Alarcon-Martinez L, Valiente-Soriano FJ, et al. Functional and morphological effects of laser-induced ocular hypertension in retinas of adult albino Swiss mice. *Mol Vis*. 2009;15:2578–2598.
27. Howell GR, Libby RT, Jakobs TC, et al. Axons of retinal ganglion cells are insulted in the optic nerve early in DBA/2J glaucoma. *J Cell Biol*. 2007;179:1523–1537.
28. Dai C, Khaw PT, Yin ZQ, Li D, Raisman G, Li Y. Structural basis of glaucoma: the fortified astrocytes of the optic nerve head are the target of raised intraocular pressure. *Glia*. 2012;60: 13–28.
29. Varela HJ, Hernandez MR. Astrocyte responses in human optic nerve head with primary open-angle glaucoma. *J Glaucoma*. 1997;6:303–313.
30. Hernandez MR. The optic nerve head in glaucoma: role of astrocytes in tissue remodeling. *Prog Retin Eye Res*. 2000;19: 297–321.
31. Neufeld AH, Liu B. Glaucomatous optic neuropathy: when glia misbehave. *Neuroscientist*. 2003;9:485–495.
32. Liu B, Chen H, Johns TG, Neufeld AH. Epidermal growth factor receptor activation: an upstream signal for transition of quiescent astrocytes into reactive astrocytes after neural injury. *J Neurosci*. 2006;26:7532–7540.
33. Johnson EC, Jia L, Cepurna WO, Doser TA, Morrison JC. Global changes in optic nerve head gene expression after exposure to elevated intraocular pressure in a rat glaucoma model. *Invest Ophthalmol Vis Sci*. 2007;48:3161–3177.
34. Balaratnasingam C, Morgan WH, Bass L, et al. Elevated pressure induced astrocyte damage in the optic nerve. *Brain Res*. 2008;1244:142–154.
35. Sun D, Lye-Barthel M, Masland RH, Jakobs TC. Structural remodeling of fibrous astrocytes after axonal injury. *J Neurosci*. 2010;30:14008–14019.
36. Johnson EC, Doser TA, Cepurna WO, et al. Cell proliferation and interleukin-6-type cytokine signaling are implicated by gene expression responses in early optic nerve head injury in rat glaucoma. *Invest Ophthalmol Vis Sci*. 2011;52:504–518.
37. Howell GR, Macalinao DG, Sousa GL, et al. Molecular clustering identifies complement and endothelin induction as early events in a mouse model of glaucoma. *J Clin Invest*. 2011;121:1429–1444.
38. Lye-Barthel M, Sun D, Jakobs TC. Morphology of astrocytes in a glaucomatous optic nerve. *Invest Ophthalmol Vis Sci*. 2013; 54:909–917.
39. Tehrani S, Johnson EC, Cepurna WO, Morrison JC. Astrocyte processes label for filamentous actin and reorient early within the optic nerve head in a rat glaucoma model. *Invest Ophthalmol Vis Sci*. 2014;55:6945–6952.
40. Crish SD, Sappington RM, Inman DM, Horner PJ, Calkins DJ. Distal axonopathy with structural persistence in glaucomatous neurodegeneration. *Proc Natl Acad Sci U S A*. 2010;107: 5196–5201.
41. Chen H, Wei X, Cho KS, et al. Optic neuropathy due to microbead-induced elevated intraocular pressure in the mouse. *Invest Ophthalmol Vis Sci*. 2011;52:36–44.
42. Nolte C, Matyash M, Pivneva T, et al. GFAP promoter-controlled EGFP-expressing transgenic mice: a tool to visualize astrocytes and astrogliosis in living brain tissue. *Glia*. 2001;33:72–86.
43. Emsley JG, Macklis JD. Astroglial heterogeneity closely reflects the neuronal-defined anatomy of the adult murine CNS. *Neuron Glia Biol*. 2006;2:175–186.

Investigative Ophthalmology & Visual Science

44. Cone FE, Gelman SE, Son JL, Pease ME, Quigley HA. Differential susceptibility to experimental glaucoma among 3 mouse strains using bead and viscoelastic injection. *Exp Eye Res*. 2010;91:415–424.
45. Sun D, Qu J, Jakobs TC. Reversible reactivity by optic nerve astrocytes. *Glia*. 2013;61:1218–1235.
46. Longair MH, Baker DA, Armstrong JD. Simple neurite tracer: open source software for reconstruction, visualization and analysis of neuronal processes. *Bioinformatics*. 2011;27: 2453–2454.
47. Ramirez AI, Salazar JJ, de Hoz R, et al. Quantification of the effect of different levels of IOP in the astroglia of the rat retina ipsilateral and contralateral to experimental glaucoma. *Invest Ophthalmol Vis Sci*. 2010;51:5690–5696.
48. Gallego BI, Salazar JJ, de Hoz R, et al. IOP induces upregulation of GFAP and MHC-II and microglia reactivity in mice retina contralateral to experimental glaucoma. *J Neuroinflammation*. 2012;9:92.
49. Rojas B, Gallego BI, Ramirez AI, et al. Microglia in mouse retina contralateral to experimental glaucoma exhibit multiple signs of activation in all retinal layers. *J Neuroinflammation*. 2014;11:133.
50. Gao S, Jakobs TC. Mice homozygous for a deletion in the glaucoma susceptibility locus INK4 show increased vulnerability of retinal ganglion cells to elevated intraocular pressure. *Am J Pathol*. 2016;186:985–1005.
51. May CA, Mittag T. Optic nerve degeneration in the DBA/2NNia mouse: is the lamina cribrosa important in the development of glaucomatous optic neuropathy? *Acta Neuropathol*. 2006;111:158–167.
52. Howell GR, Walton DO, King BL, Libby RT, John SW. Datgan, a reusable software system for facile interrogation and visualization of complex transcription profiling data. *BMC Genomics*. 2011;12:429.
53. Anderson MG, Libby RT, Gould DB, Smith RS, John SW. High-dose radiation with bone marrow transfer prevents neurodegeneration in an inherited glaucoma. *Proc Natl Acad Sci U S A*. 2005;102:4566–4571.
54. Howell GR, Soto I, Zhu X, et al. Radiation treatment inhibits monocyte entry into the optic nerve head and prevents neuronal damage in a mouse model of glaucoma. *J Clin Invest*. 2012;122:1246–1261.
55. Bosco A, Crish SD, Steele MR, et al. Early reduction of microglia activation by irradiation in a model of chronic glaucoma. *PLoS One*. 2012;7:e43602.
56. Johnson EC, Cepurna WO, Choi D, Choe TE, Morrison JC. Radiation pretreatment does not protect the rat optic nerve from elevated intraocular pressure-induced injury. *Invest Ophthalmol Vis Sci*. 2015;56:412–419.
57. Soto I, Howell GR. The complex role of neuroinflammation in glaucoma. *Cold Spring Harb Perspect Med*. 2014;4:a017269.
58. Cone FE, Steinhart MR, Oglesby EN, Kalesnykas G, Pease ME, Quigley HA. The effects of anesthesia, mouse strain and age on intraocular pressure and an improved murine model of experimental glaucoma. *Exp Eye Res*. 2012;99:27–35.
59. Li R, Liu JH. Telemetric monitoring of 24 h intraocular pressure in conscious and freely moving C57BL/6J and CBA/CaJ mice. *Mol Vis*. 2008;14:745–749.
60. Bushong EA, Martone ME, Jones YZ, Ellisman MH. Protoplasmic astrocytes in CA1 stratum radiatum occupy separate anatomical domains. *J Neurosci*. 2002;22:183–192.
61. Wilhelmsson U, Bushong EA, Price DL, et al. Redefining the concept of reactive astrocytes as cells that remain within their unique domains upon reaction to injury. *Proc Natl Acad Sci U S A*. 2006;103:17513–17518.
62. Nguyen JV, Soto I, Kim KY, et al. Myelination transition zone astrocytes are constitutively phagocytic and have synuclein dependent reactivity in glaucoma. *Proc Natl Acad Sci U S A*. 2011;108:1176–1181.
63. Davis CH, Kim KY, Bushong EA, et al. Transcellular degradation of axonal mitochondria. *Proc Natl Acad Sci U S A*. 2014;111:9633–9638.
64. Cooper ML, Crish SD, Inman DM, Horner PJ, Calkins DJ. Early astrocyte redistribution in the optic nerve precedes axonopathy in the DBA/2J mouse model of glaucoma. *Exp Eye Res*. 2016;150:22–23.
65. Bosco A, Breen KT, Anderson SR, Steele MR, Calkins DJ, Vetter ML. Glial coverage in the optic nerve expands in proportion to optic axon loss in chronic mouse glaucoma. *Exp Eye Res*. 2016;150:34–43.
66. Coughlin L, Morrison RS, Horner PJ, Inman DM. Mitochondrial morphology differences and mitophagy deficit in murine glaucomatous optic nerve. *Invest Ophthalmol Vis Sci*. 2015; 56:1437–1446.
67. Baltan S, Inman DM, Danilov CA, Morrison RS, Calkins DJ, Horner PJ. Metabolic vulnerability disposes retinal ganglion cell axons to dysfunction in a model of glaucomatous degeneration. *J Neurosci*. 2010;30:5644–5652.
68. Calkins DJ. Critical pathogenic events underlying progression of neurodegeneration in glaucoma. *Prog Retin Eye Res*. 2012; 31:702–719.
69. Li Y, Li D, Ying X, Khaw PT, Raisman G. An energy theory of glaucoma. *Glia*. 2015;63:1537–1552.

Investigative Ophthalmology & Visual Science